ChemComm

COMMUNICATION

View Article Online
View Journal | View Issue

Cite this: *Chem. Commun.*, 2019, 55, 12996

Received 21st August 2019,
Accepted 3rd October 2019

DOI: 10.1039/c9cc06485k

rsc.li/chemcomm

Etchable SERS nanosensor for accurate pH and hydrogen peroxide sensing in living cells†

Lu Bai,[a] Xiaojie Wang,[b] Kaifu Zhang,[a] Xiaoyue Tan,[b] Yuying Zhang *[b] and Wei Xie[a]

No methodology has been built to distinguish intracellular SERS nanosensors from cell outer membrane bound-ones. Here we propose a "turning off" strategy by combining etchable SERS nanosensors with a non-permeable etchant. The SERS signals outside the living cells can be rapidly removed, leaving only the internalized nanosensors for imaging and thereby allowing accurate intracellular pH and H_2O_2 sensing.

Intracellular microenvironment sensing in living cells is of vital importance for understanding various physiological and pathological processes.[1–3] As an ultra-sensitive and non-destructive spectroscopic technology, surface-enhanced Raman spectroscopy (SERS) has been extensively applied to live cell studies.[4–8] One of its most important applications is SERS-based microenvironment sensing in living cells using SERS nanosensors, which typically consist of a metal nanoparticle (NP, usually gold or silver) as a SERS substrate, reporter molecules with both strong Raman signal and sensitive chemical response on the NP surface, and a protective shell (usually using materials such as SH-PEG, PVP, silica and BSA).[9–11] Until now, SERS nanosensors have been widely applied for the characterization of intracellular microenvironmental indicators, such as intracellular pH, hydrogen peroxide (H_2O_2), nitric oxide (NO), hydrogen sulfide (H_2S), *etc.*[12–21] When nanosensors are exposed to cultured cells, most of them are internalized into the cells through endocytosis. However, it is frequently observed that a portion of the NPs adsorb non-specifically on cell outer membranes or culture plates, and cannot be removed even through harsh washing.[22] The extracellular NPs produce unwanted signals during the imaging process, which induce ambiguous detection results. Therefore, setting up a method to discriminate internalized NPs from cell surface-bound ones is of pivotal importance for getting accurate intracellular information.

Thus, as shown in Scheme 1, we developed an etchable SERS nanosensor that enables turning "off" the signals outside the cells upon adding an etching solution. Au@Ag core–shell NPs were used as SERS substrates, since they are highly plasmonic-active and less cytotoxic compared with silver NPs. When a hexacyanoferrate-thiosulphate etching solution is added, the silver shells of the NPs are dissolved, and the Raman reporter molecules attached on the NP surface are released and lose their Raman enhancement. Most importantly, ferricyanide [$Fe(CN)_6^{3-}$] and thiosulfate ($S_2O_3^{2-}$) cannot facilely pass through the living cell membrane,[23] hence the internalized NPs are effectively protected from etching and only the extracellular NPs are cleared.

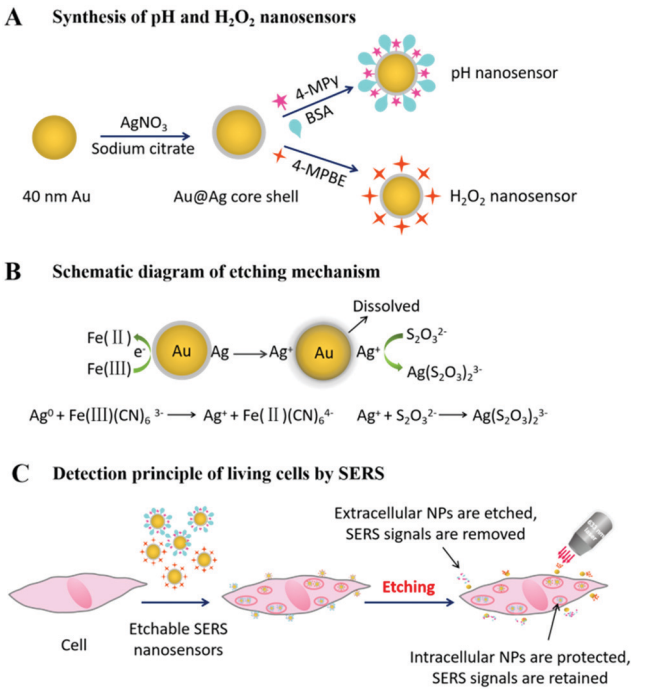

Scheme 1 (A) Synthesis of etchable SERS nanosensors. (B) The etching mechanism. (C) SERS detection of living cells.

[a] *Key Laboratory of Advanced Energy Materials Chemistry, College of Chemistry, Nankai University, Tianjin 300071, China*
[b] *Medical School of Nankai University, Tianjin 300071, China. E-mail: Yuyingzhang@nankai.edu.cn*

† Electronic supplementary information (ESI) available: Experimental procedures and supporting figures. See DOI: 10.1039/c9cc06485k

In demonstration of this SERS-etchant combination technique, we fabricated a SERS pH nanosensor using 4-mercaptopyridine (4-MPy) as the probe molecule, and BSA was coated on the surface to improve the NP stability and biocompatibility. The etchable Au@Ag-(4-MPy)-BSA (AMBA) pH nanosensors have been successfully used for accurate intracellular pH sensing of single living cells, without any disturbance from extracellular signals. We further extend this method to intracellular H_2O_2 sensing in living cells based on 4-mercaptophenylboronic ester (4-MPBE)-modified Au@Ag NPs (AMPE H_2O_2 nanosensors).

Fabrication of an intact silver shell around the gold core is the key for the complete clearance of the strong SERS signal outside the cells. If the gold core is not completely wrapped with a silver shell, the exposed gold surface will also be modified with probe molecules, and cause redundant SERS signal when the NPs adhere to the cell membrane or culture dish even after etching. We first synthesized gold seeds with an average diameter of ~40 nm (Fig. S1A, ESI†), and then grew a silver shell around the gold core. Compared to the Au seeds, the extinction peak of the Au@Ag core–shell NPs blue shifted from ~529 nm to ~421 nm (Fig. S1C, ESI†), indicating that a silver shell formed around the gold core. Fig. 1A shows the TEM image of the Au@Ag core–shell NPs (~50 nm) and EDX elemental maps of Au and Ag, respectively. It is palpable that the silver shell completely coated the gold core with an average thickness of ~5 nm. The silver shell can be etched by an etchant consisting of ferricyanide that oxidizes Ag^0 to Ag^+ and thiosulfate that clears newly formed silver ions, as shown in Scheme 1B. The appropriate etching conditions were optimized, as illustrated in Fig. S2 (ESI†). 1 mM etchant and 5 min were chosen as the optimal etching conditions since the complete dissolution of the silver shell was judged by the visual inspection of the solution colour and the vanished SERS signals. In the TEM image of the remnant NPs after etching with 1 mM etchant for 5 min, we found that the silver shells were completely dissolved and a slight aggregation of the residual gold cores occurred (Fig. S1B, ESI†). The extinction peak of the remnant NPs has red shifted to ~536 nm (similar to original Au seeds, ~529 nm), suggesting the complete dissolution of the silver shells and a slight aggregation of the NPs, which agrees well with the TEM image.

We chose 4-MPy as a pH probe molecule because it is a kind of bifunctional molecule with a thiol group strongly binding to plasmonic metal NPs and a pyridine group sensitively responding to pH changes. The BSA modification functioned as a protective layer.[10] Fig. S3A (ESI†) shows the UV-Vis extinction spectra of the prepared AMBA pH nanosensors. Compared to the Au@Ag nanoshells, the modification of 4-MPy and BSA caused a slight red shift of the peak from ~421 nm to ~428 nm, suggesting successful combination of the molecules with the NPs. From the SERS spectra presented in Fig. S3B (ESI†), we can find several characteristic peaks of the pyridyl group (as listed in Table S1, ESI†).[24] The high signal/noise ratio benefited from the strong SERS plasmonic enhancement activity of the Au@Ag core–shell NPs, and the nanosensors exhibited a good stability even after storage for 7 days. Fig. 1B shows the normalized SERS spectra of the AMBA pH nanosensors in PBS solutions of various pH values ranging from pH 4.6 to 8.4. The intensity of the peak at 1577 cm^{-1} increased and that at 1614 cm^{-1} decreased with the rise of pH value. As shown in Fig. 1C, the peaks at 1577 and 1614 cm^{-1} represent the different ionization states of the pyridine group. When the pH value increased, the degree of ionization of the pyridyl group reduced, resulting in an increased intensity of the peak at 1577 cm^{-1} and a decreased intensity of the peak at 1614 cm^{-1}.[24] Consequently, the peaks at 1577 and 1614 cm^{-1} were chosen for pH sensing. We found that the intensity ratio of the peaks at 1577 and 1614 cm^{-1} changed with the pH values exponentially, as shown in Fig. 1C. The pH standard curve exhibited a good correlation and a small standard deviation (R^2 = 0.996), indicating an accurate pH response.

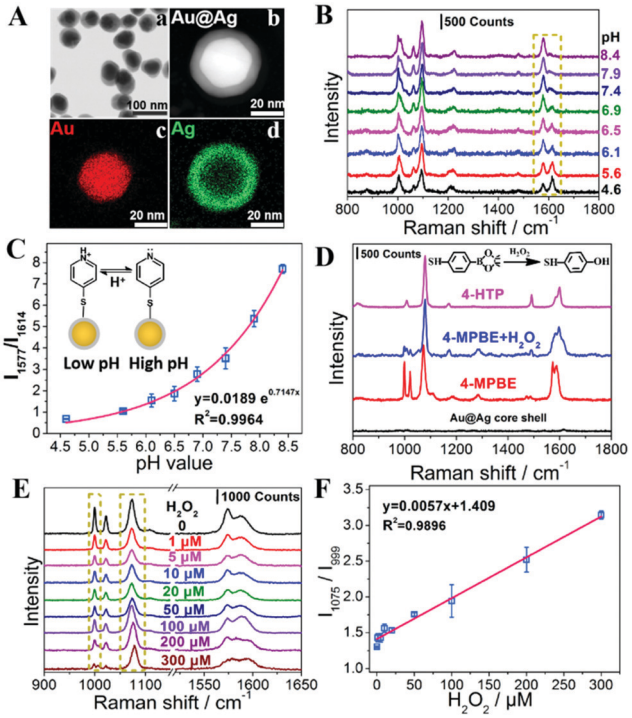

Fig. 1 (A) TEM image (a) and DF-STEM image (b) of Au@Ag core–shell NPs, and EDX elemental maps of Au (c) and Ag (d), respectively. (B) The normalized SERS spectra of AMBA pH nanosensors in PBS solutions of various pH values ranging from pH 4.6 to 8.4. (C) pH standard curve of the AMBA pH nanosensors, obtained from the intensity ratio of the peaks at 1577 and 1614 cm^{-1}. (D) SERS spectra of Au@Ag core–shell NPs, AMPE H_2O_2 nanosensors, AMPE H_2O_2 nanosensors with treatment of H_2O_2 and Au@Ag-(4-HTP) NPs. (E) SERS spectra of the AMPE H_2O_2 nanosensors in the presence of 0–300 μM of H_2O_2 in PBS solution. (F) SERS response of the AMPE H_2O_2 nanosensors in PBS solution as a function of H_2O_2 concentration, obtained from the intensity ratio of the peaks at 1075 and 999 cm^{-1}.

The AMBA pH nanosensors were further applied to detect the intracellular pH of living MCF-10A cells. Typically, after co-incubation with cultured cells, the pH nanosensors are swallowed into the endosomes of the cell through the endocytosis process, and they sense the pH close to neutral (6.0–7.5) in early endosomes and acidic (4.5–6.0) in late endosomes or lysosomes.[25] As expected, the nanosensors were ingested by the cell after a 4 h-co-incubation and exhibited a high SERS intensity in the cell region; the detected

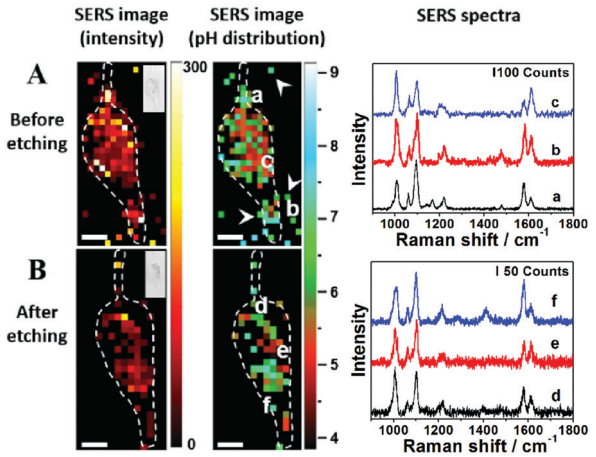

Fig. 2 SERS images of a MCF-10A cell incubated with pH nanosensors for 4 h before (A) and after etching (B), using the peak of 4-MPy at 1577 cm^{-1} and the intensity ratio I_{1577}/I_{1614}, and typical SERS spectra obtained from different locations of the cell (insets: bright field images). Scale bar: 10 μm.

intracellular pH values varied from 4.0 to 7.5 depending on the location of the nanosensors (in early endosomes/late endosomes/lysosomes).[25] However, some NPs bound to the cell membrane or adhered to the dish, which cannot be removed by rinsing (Fig. 2A, white arrows), emit unwanted SERS signals outside the cells and affect the pH of the culture medium (detected pH values ~7.5). Several typical SERS spectra obtained from diverse locations were presented, showing different intensity ratios (I_{1577}/I_{1614}), which indicate varied pH values. To eliminate the interference from the signals outside the cell, an etching procedure (1 mM etchant, 5 min) was carried out. The NPs adhering to the dish or bound to the cell membrane were dissolved, while the intracellular NPs were protected. As shown in Fig. 2B, the SERS signals outside the cells completely disappeared after etching while the intracellular signals remained, and at the same time the overall SERS intensity reduced to some extent. No obvious change in the morphology of the cells was observed (Fig. 2 insets and Fig. S4, ESI†), revealing that only negligible damage was caused by the etching process. The experiment was repeated more than 3 times, and another example is given in Fig. S5 (ESI†). These results indicated that the intracellular pH can be detected more precisely using the AMBA pH nanosenor combined with an etching process compared with previous procedures.

We also monitored the etching of extracellular NPs using correlative dark field-SERS microscopy. As shown in the dark field images (Fig. S6, ESI†), there were a large number of NPs distributing not only inside but also outside the cell before etching. In the correlative SERS mapping images, corresponding SERS signals were detected in the region both inside and outside the cells. While after etching, only the intracellular NPs can be observed, demonstrating the selectivity and effectiveness of the etching procedure.

We further extended this method to the detection of H_2O_2. 4-MPBE was chosen as the H_2O_2 probe molecule owing to its unique boronate-to-phenol conversion oxidized by H_2O_2. Fig. S3C (ESI†) shows the UV-Vis extinction spectra of the prepared AMPE H_2O_2 nanosensors. The slight red shift of the peak indicates the modification of the 4-MPBE molecules on the Au@Ag core–shell NPs. From the SERS spectra of 4-MPBE in Fig. 1D, we can find several characteristic peaks of the boronate ester group and benzene ring,[18] as listed in Table S2 (ESI†). When 300 μM of H_2O_2 was added to oxidize the boronate ester group, the peak intensity at 999 and 1021 cm^{-1} decreased significantly and the SERS spectrum after oxidization was almost in concert with that of 4-hydroxythiophenol (4-HTP). The H_2O_2 response of the AMPE nanosensors was evaluated in PBS solution by adding H_2O_2 of different concentrations. Fig. 1E shows the SERS spectra of the AMPE H_2O_2 nanosensors in the presence of 0–300 μM H_2O_2. It is apparent that the peak intensity at 999 cm^{-1} gradually reduced with the increasing concentration of H_2O_2 while that at 1075 cm^{-1} was nearly constant. Accordingly, we used the intensity ratio of the two peaks at 999 and 1075 cm^{-1} as an indicator of the H_2O_2 concentration. The linear relationship between the intensity ratio (I_{1075}/I_{999}) and the concentration of H_2O_2 is shown in Fig. 1F, with a detection limit of 450 nM based on a signal-to-noise ratio of S/N = 3. The high correlation coefficient and petty standard deviation (R^2 = 0.9896) of the standard curve illustrated the accuracy and feasibility of the AMPE H_2O_2 nanosensors for quantitative detection of H_2O_2.

The AMPE H_2O_2 nanosensors were subsequently used to detect the intracellular concentration of H_2O_2. SKBR-3 cells were incubated with the nanosensors for 4 h, and then SERS images were recorded and analyzed. As shown in Fig. 3A, strong

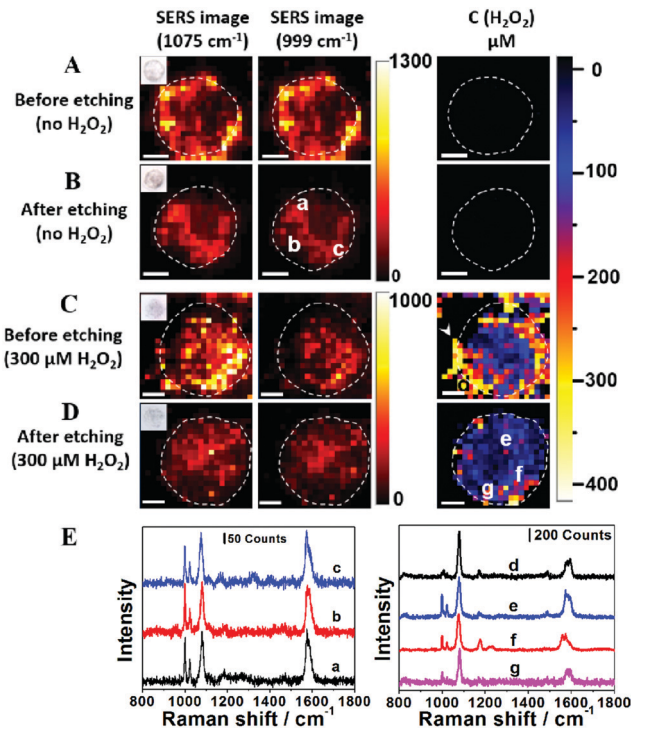

Fig. 3 SERS images of SKBR-3 cells incubated with AMPE H_2O_2 nanosensors for 4 h before (A and C) and after (B and D) etching, using the peak intensity of 999 and 1075 cm^{-1} of the 4-MPBE molecule (insets: bright field images). The cells were treated without (A and B) or with (C and D) 300 μM of H_2O_2. (E) Typical SERS spectra obtained from different locations of the cell as indicated in B, C and D. Scale bar: 5 μm.

SERS signals were detected both inside and outside the cell membrane; while after an etching procedure to remove the extracellular nanosensors (Fig. 3B), a portion of the SERS signals disappeared, and the peak intensity obviously decreased. Almost equal intensities of the peaks at 999 and 1075 cm^{-1} were obtained in the SERS images, indicating a very low level of H_2O_2 in the cell. The typical SERS spectra in different locations of the cell after etching are shown in Fig. 3E, which are similar to that obtained in PBS solution without H_2O_2 (as shown in Fig. 1E). In contrast, when the cells were treated with 300 μM of H_2O_2, the intensity of the peak at 999 cm^{-1} decreased significantly, showing an elevated H_2O_2 level. The intracellular H_2O_2 concentration was calculated by the conversion of the intensity ratio (I_{1075}/I_{999}) *versus* H_2O_2 concentration according to the above standard curve, and presented in the right column of Fig. 3A–D. Notably, the concentration distribution of H_2O_2 in the cell is totally different before and after etching: before etching, the nanosensors surrounding the cell membrane sense a much higher concentration of H_2O_2 than the ones inside the cell (Fig. 3C, white arrow in the right picture); while after etching, the concentration of H_2O_2 is almost uniform across the whole cell (Fig. 3D, right). An average value of H_2O_2 concentration is calculated to be 253.78 μM and 105.94 μM before and after etching, respectively. The marked difference arose from the redundant SERS nanosensors outside the cell, which can contact with more H_2O_2 molecules in the culture medium and be oxidized to a larger extent than the intracellular ones. And an etching step can thoroughly remove these NPs and eliminate the interfering signals. Fig. 3E shows the typical SERS spectra of different locations outside or inside the cells as indicated in Fig. 3C and D. The distinct intensity ratio (I_{1075}/I_{999}) represented various concentrations of H_2O_2. Another example is presented in Fig. S8 (ESI†). These results demonstrated that the AMPE H_2O_2 nanosensors can be successfully applied for the precise detection of the intracellular H_2O_2 with the cooperation of the etchant.

We also evaluated the cytotoxicity of the AMBA pH nanosensors and AMPE H_2O_2 nanosensors using the MTT assay. As shown in Fig. S9 (ESI†), no obvious toxicity was observed with the addition of different doses of the pH or H_2O_2 nanosensors and etching for 5 minutes, even at a NP concentration as high as 225 pM. In contrast, the cell viability decreases severely when Ag NPs (50 nm) were used as SERS substrates. These results suggested the excellent biocompatibility of the nanosensors using the Au@Ag core–shell NPs as SERS substrates.

In conclusion, in order to avoid disturbing signals resulting from the nanosensors bound to the cell membrane or adhering on the culture dish in SERS imaging, we propose a ''turning off'' strategy by combining etchable SERS nanosensors with a non-permeable etchant. Au@Ag core–shell NPs were used as the SERS substrates, on which the silver shells can be etched by an innoxious hexacyanoferrate-thiosulphate redox-based solution and thereby eliminates the unwanted SERS signals. We synthesized etchable AMBA pH nanosensors with a sensitive pH response ranging from pH 4.6 to 8.4. It was successfully applied to the accurate detection of the intracellular pH value. In addition, we prepared etchable AMPE H_2O_2 nanosensors with high sensitivity and low cytotoxicity, which can quantitatively monitor the H_2O_2 level precisely in living cells. By eliminating the interference caused by extracellular NPs, the etchable SERS nanosensors can potentially be modified with other probe molecules for the accurate detection of different signal molecules in living cells, and even for SERS imaging of tissues, organs, and living organisms.

The authors would like to acknowledge the financial support from National Natural Science Foundation of China (81871487 and 21775074).

Conflicts of interest

There are no conflicts to declare.

Notes and references

1 Y. J. Lee, H. C. Kang, J. Hu, J. W. Nichols, Y. S. Jeon and Y. H. Bae, *Biomacromolecules*, 2012, **13**, 2945.
2 M. T. Lin and M. F. Beal, *Nature*, 2006, **443**, 787.
3 N. Houstis, E. D. Rosen and E. S. Lander, *Nature*, 2006, **440**, 944.
4 K. Kneipp, Y. Wang, H. Kneipp, L. T. Perelman, I. Itzkan, R. R. Dasari and M. S. Feld, *Phys. Rev. Lett.*, 1997, **78**, 1667.
5 C. Krafft, M. Schmitt, I. W. Schie, D. Cialla-May, C. Matthäus, T. Bocklitz and J. Popp, *Angew. Chem., Int. Ed.*, 2017, **56**, 4392.
6 Y. Zhang, X. Mi, X. Tan and R. Xiang, *Theranostics*, 2019, **9**, 491.
7 S. Hennig, V. Mönkemöller, C. Böger, M. Müller and T. Huser, *ACS Nano*, 2015, **9**, 6196.
8 Q. Dong, X. Wang, X. Hu, L. Xiao, L. Zhang, L. Song, M. Xu, Y. Zou, L. Chen, Z. Chen and W. Tan, *Angew. Chem., Int. Ed.*, 2018, **57**, 711.
9 L. A. Lane, X. Qian and S. Nie, *Chem. Rev.*, 2015, **115**, 10489.
10 X. S. Zheng, P. Hu, Y. Cui, C. Zong, J. M. Feng, X. Wang and B. Ren, *Anal. Chem.*, 2014, **86**, 12250.
11 K. Malek, A. Krolikowska and J. Bukowska, *J. Phys. Chem. B*, 2014, **118**, 4025.
12 C. E. Talley, L. Jusinski, C. W. Hollars, S. M. Lane and T. Huser, *Anal. Chem.*, 2004, **76**, 7064.
13 A. Jaworska, L. E. Jamieson, K. Malek, C. J. Campbell, J. Choo, S. Chlopicki and M. Baranska, *Analyst*, 2015, **140**, 2321.
14 W. Ji, N. Spegazzini, Y. Kitahama, Y. Chen, B. Zhao and Y. Ozaki, *J. Phys. Chem. Lett.*, 2012, **3**, 3204.
15 Y. Shen, L. Liang, S. Zhang, D. Huang, J. Zhang, S. Xu, C. Liang and W. Xu, *Nanoscale*, 2018, **10**, 1622.
16 X. S. Zheng, C. Zong, X. Wang and B. Ren, *Anal. Chem.*, 2019, **91**, 8383.
17 X. Gu, H. Wang, Z. D. Schultz and J. P. Camden, *Anal. Chem.*, 2016, **88**, 7191.
18 R. Peng, Y. Si, T. Deng, J. Zheng, J. Li, R. Yang and W. Tan, *Chem. Commun.*, 2016, **52**, 8553.
19 K. Cui, C. Fan, G. Chen, Y. Qiu, M. Li, M. Lin, J. B. Wan, C. Cai and Z. Xiao, *Anal. Chem.*, 2018, **90**, 12137.
20 Q. Xu, W. Liu, L. Li, F. Zhou, J. Zhou and Y. Tian, *Chem. Commun.*, 2017, **53**, 1880.
21 D. W. Li, L. L. Qu, K. Hu, Y. T. Long and H. Tian, *Angew. Chem., Int. Ed.*, 2015, **54**, 12758.
22 G. B. Braun, T. Friman, H. B. Pang, A. Pallaoro, T. H. Mendoza, A. M. A. Willmore, V. R. Kotamraju, A. P. Mann, Z. G. She, K. N. Sugahara, N. O. Reich, T. Teesalu and E. Ruoslahti, *Nat. Mater.*, 2014, **13**, 904.
23 D. Koley and A. J. Bard, *Proc. Natl. Acad. Sci. U. S. A.*, 2010, **107**, 16783.
24 H. Z. Yu, N. Xia and Z. F. Liu, *Anal. Chem.*, 1999, **71**, 1354.
25 K. L. Nowak-Lovato and K. D. Rector, *Appl. Spectrosc.*, 2009, **63**, 387.